Supplementary Information

for

Giant shift upon strain on the fluorescence spectrum of V_NN_B color centers in h-BN

Song Li, Jyh-Pin Chou, and Alice Hu
Department of Mechanical Engineering, City University of Hong Kong, Hong Kong SAR, China

Martin B. Plenio
Institute of Theoretical Physics and IQST, Albert-Einstein-Allee 11, Ulm University, 89069 Ulm, Germany

Péter Udvarhelyi
Wigner Research Centre for Physics, P.O. Box 49, H-1525 Budapest, Hungary and
Eötvös Science University, Pázmány Péter Sétány 1/A, H-1117 Budapest, Hungary

Gergő Thiering
Wigner Research Centre for Physics, P.O. Box 49, H-1525 Budapest, Hungary

Mehdi Abdi
Department of Physics, Isfahan University of Technology, Isfahan 84156-83111, Iran

Adam Gali
Wigner Research Centre for Physics, P.O. Box 49, H-1525 Budapest, Hungary and
Budapest University of Technology and Economics, Budafoki út 8, H-1111 Budapest, Hungary
(Dated: August 16, 2020)

SUPPLEMENTARY NOTE 1: POINT SYMMETRY OF THE DEFECT

The V_NN_B defect has C_{2v} symmetry when it assumes a planar configuration in the xy plane of the monolayer h-BN (see Fig. 2(a) in the main text). The C_2 rotation axis lies along the y axis, one mirror plane $\sigma_v(xy)$ is in the plane of the monolayer and another $\sigma_v(yz)$ is perpendicular to it. The labeling of the defect orbitals follow thier transformation properties according to the irreducible representations of the C_{2v} point group (see Supplementary Table 1).

The ground state of the defect shows vibronic instability leading to a lowering of its C_{2v} symmetry to its subgroup C_s in this state. As the instability is caused by perpendicular (B_2) phonon modes, the resulted perturbation in the defect geometry and orbitals has the same (perpendicular) symmetry, defining the $\sigma(yz)$ mirror plane in C_s symmetry (see Supplementary Table 2).

The irreducible representation of the perturbed defect states can be assigned by following the subgroup correlation in Supplementary Table 3, they all belong to A' irreducible representation. In the lowered symmetry configuration, the orbitals are closely related to their high symmetry counterparts, thus we keep the high symmetry labels for the sake of simplicity.

Supplementary Table 1: Character table of the C_{2v} point group.

	E	$C_2(y)$	$\sigma_v(xy)$	$\sigma_v(yz)$
A_1	1	1	1	1
A_2	1	1	-1	-1
B_1	1	-1	1	-1
B_2	1	-1	-1	1

Supplementary Table 2: Character table of the C_s point group.

	E	$\sigma(yz)$
A'	1	1
A''	1	-1

Supplementary Table 3: Subgroup correlation table of the C_{2v} point group. The columns show the effect of symmetry lowering on the high symmetry irreducible representations.

group	irreducible representations			
C_{2v}	A_1	A_2	B_1	B_2
$C_s(yz)$	A'	A''	A''	A'

SUPPLEMENTARY NOTE 2: OPTICAL TRANSITION AS A FUNCTION OF DEFECT CONFIGURATIONS

To compare the possibility and intensity of the two excitation schemes, the transition dipole moment is calculated as shown in Supplementary Figure 1. The imaginary part of the dielectric function of the ground state configuration is used to do analysis. The two excitation peaks could be identified based on the energy differences between Kohn-Sham orbitals. Compared with C_{2v} configuration in Supplementary Figure 1(b), the dipole moment of $A_1 \leftrightarrow B_2$ transition with C_s configuration changes from the out-of-plane (z) direction to in-plane direction (y). In addition, the relative intensity is larger than that of the $B_2 \leftrightarrow B_2$ transition. Also, we find that the intensity of the optical transition dipole moment could be tuned through external strain. Tensile strain along perpendicular direction or compressive strain along parallel direction will strengthen the intensity of the $A_1 \leftrightarrow B_2$ transition while the opposite strain will enhance the $B_2 \leftrightarrow B_2$ transition.

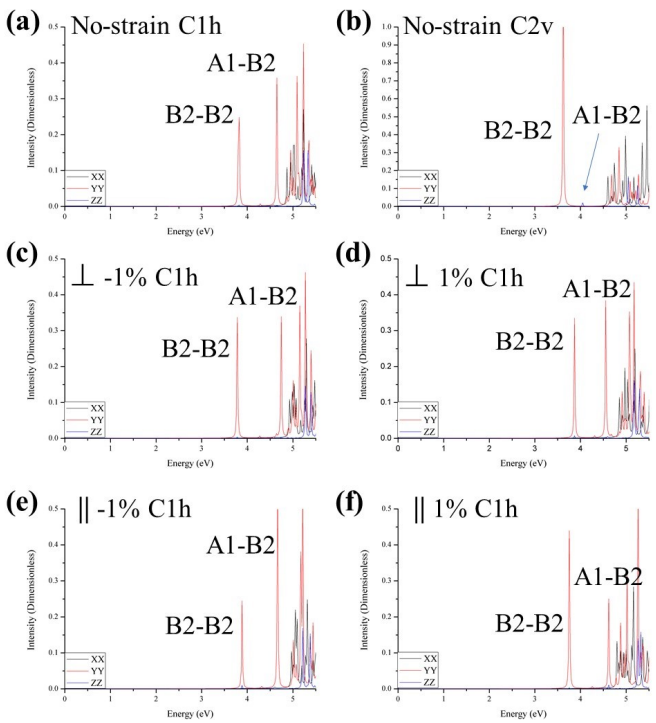

Supplementary Figure 1: The dielectric function matrix of the two excitation schemes under different symmetry and external strain. XX and YY correspond to perpendicular ($\perp$) and parallel ($\parallel$) directions, respectively. The dielectric function at (a) C_s and C_{2v} symmetry without strain. The dielectric function at C_s symmetry with (c) -1% and (d) 1% strain along $\perp$ direction. The dielectric function at C_s symmetry with (e) -1% and (f) 1% strain along $\parallel$ direction.

SUPPLEMENTARY NOTE 3: STRAIN DEPENDENCE OF $B_2 \leftrightarrow B_2'$ OPTICAL TRANSITION

Supplementary Figure 2(a) depicts the strain dependence of the $B_2 \leftrightarrow B_2'$ optical transition which shows a strong non-linearity for the applied strain in parallel direction. As can be inferred from Supplementary Figure 2(c) this is associated with the non-linear strain dependence of the occupied b_2' level in the excited state electronic configuration, where the two Jahn-Teller distorted b_2 and b_2' defect states strongly interact.

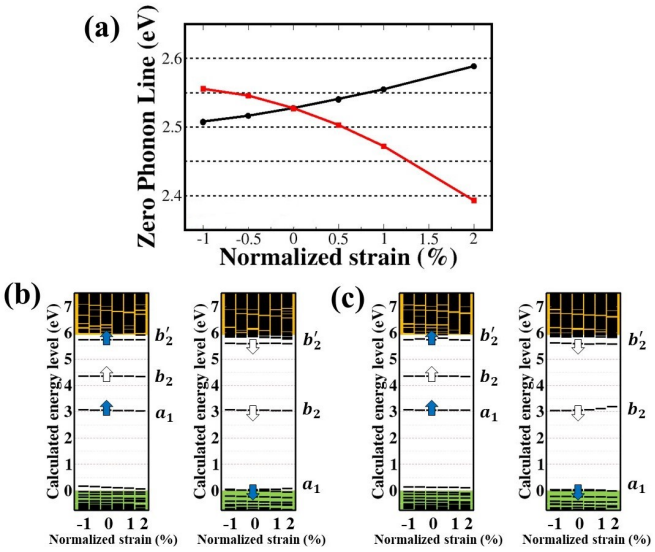

Supplementary Figure 2: (a) The ZPL shift of $B_2 \leftrightarrow B_2'$ transition with perpendicular (black) and parallel (red) directions. The energy level at excited state (b_2 to b_2' transition) with C_s symmetry evolution as a function of external strain for (b) perpendicular ($\perp$) and (c) parallel ($\parallel$) directions, respectively.

SUPPLEMENTARY NOTE 4: PHONON MODES OF $V_N N_B$ IN MONOLAYER AND BULK STRUCTURES

Supplementary Figure 3 shows the phonon mode of the defect. Generally, it is dominated by the substitutional nitrogen atom. The displacement of the two boron atoms are too small to show with vectors, we speculate the wrinkle motion of the boron atoms are to match the displacement of nitrogen. Supplementary Tables 4 and 5 list the displacement of the relevant atoms in monolayer and bulk models, respectively. The absolute displacement of the defect in monolayer is larger than it in the bulk due to the van der Waals interaction.

Supplementary Table 4: The displacement components of the nearest atoms along three directions with monolayer model. Abs. is the absolute value. The unit is in Å.

Atom	x	y	z	Abs.
N	0	0.035	-0.599	0.600
B1	0.014	0.022	0.045	0.052
B2	-0.014	0.022	0.045	0.052

Supplementary Table 5: The displacement components of the nearest atoms along three directions with bulk model. Abs. is the absolute value. The unit is in Å.

Atom	x	y	z	Abs.
N	0	0.038	-0.423	0.425
B1	0.012	0.020	0.051	0.056
B2	-0.012	0.020	0.051	0.056

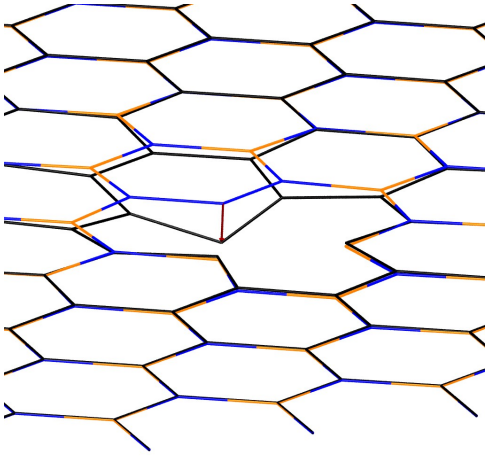

Supplementary Figure 3: The phonon mode of the $V_NN_B$defect on monolayer h-BN.The red arrow indicates the direction of phonon mode of the defect. The mode of the two boron atoms is negligible compared to the nitrogen atom.

SUPPLEMENTARY NOTE 5: RADIATIVE LIFETIME OF THE $A_1 \leftrightarrow B_2$ TRANSITION

The radiative lifetime of the excited state of the defect can be calculated as

$$\frac{1}{\tau} = \frac{n\omega^3 |\mu|^2}{3\pi\epsilon_0}, \quad (1)$$

where n refers to the refractive index of h-BN and $\hbar\omega$ is the excitation energy. μ represents the optical transition dipole moment between the ground and excited states, and ϵ_0 is the dielectric constant. μ is calculated within the independent particle approximation, i.e., between the DFT Kohn-Sham levels in the ground state geometry. The calculated lifetime of $A_1 \leftrightarrow B_2$ transition is 49.8 ns. This corresponds about two orders of magnitude faster rate than the calculated tunneling rate (see main text).

SUPPLEMENTARY NOTE 6: ZPL AND ELECTRON-COUPLING ON BULK h-BN

To confirm the result on monolayer is also valid for h-BN multilayers, we carried out the same calculation on bulk h-BN model, with the defect located at the middle layer. The relaxed structure has interlayer distance about 3.37 Å. After optimization, we find the buried defect still prefers the C_s symmetry, as shown in Supplementary Figure 4(a). However, the interlayer van der Waals interaction suppresses the magnitude of the distortion a bit: the out-of-plane displacement of the nitrogen substitutional atom is 0.42 Å, which is smaller than that in the monolayer (0.60 Å). The resulting relaxation energy is about 50.5 meV going from the C_{2v} symmetry to the low C_s symmetry.

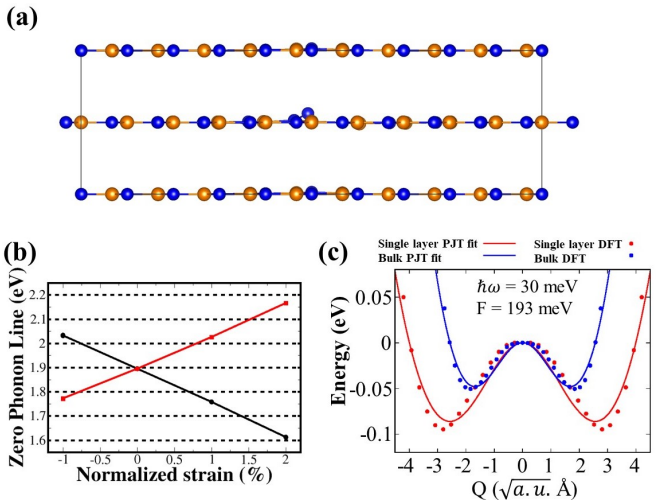

Supplementary Figure 4: (a) Side view of the bulk model of h-BN. The V_NN_B defect is buried with a perfect layer. (b) The ZPL evolution as a function of external strain for a_1 to b_2 transition. The black and red line denote the directions of strain perpendicular ($\perp$) and parallel ($\parallel$) directions.(c) The calculated APES of the $^2B_2$ ground state. The result of monolayer model is depicted as comparison. The resultant values of bulk model are F=193 meV and $\hbar\omega$=30 meV.

In Supplementary Figure 4(b) we depict the results of the calculated ZPLs as a function of strain in bulk h-BN. The ZPL of no-strain structure is 1.895 eV which is very close to the monolayer result at 1.90 eV. As expected, the interlayer interaction has little effect on the ZPL's evolution under strain. The ZPL shows blueshift (redshift) under strain along parallel (perpendicular) directions. At $[-1;+2]$% range, the energy difference of ZPLs between the bulk and the monolayer structures is less than 0.01 eV. Therefore, the quantum emission of V_NN_B

defect in bulk structure is robust. Since the displacement of substitutional nitrogen atom in bulk is smaller than that in the monolayer, the electron-phonon coupling also changes. The APES of $^2B_2$ ground state of $V_N N_B$ in the bulk structure has a narrower curve than that in the monolayer. Consequently, the electron-coupling strength is at F=193 meV and the effective frequency is at $\hbar\omega$=30 meV.